





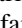







**Resolving vibrations in a polyatomic molecule with femtometer precision via x-ray spectroscopy**Patrick Rupprecht <sup>1,\*</sup>, Lennart Aufleger <sup>1</sup>, Simon Heinze <sup>2</sup>, Alexander Magunia <sup>1</sup>, Thomas Ding <sup>1</sup>, Marc Rebholz <sup>1</sup>, Stefano Amberg <sup>1</sup>, Nikola Mollov <sup>1</sup>, Felix Henrich <sup>1</sup>, Maurits W. Haverkort <sup>2</sup>, Christian Ott <sup>1,†</sup> and Thomas Pfeifer <sup>1,‡</sup><sup>1</sup>Max-Planck-Institut für Kernphysik, Saupfercheckweg 1, 69117 Heidelberg, Germany<sup>2</sup>Institut für Theoretische Physik, Ruprecht-Karls-Universität Heidelberg, Philosophenweg 19, 69120 Heidelberg, Germany

(Received 15 April 2022; revised 17 May 2023; accepted 5 September 2023; published 27 September 2023)

We measure molecular vibrations with femtometer precision via resonance energy shifts using time-resolved x-ray absorption spectroscopy. For a demonstration, a Raman process excites the  $A_{1g}$  mode in gas-phase  $\text{SF}_6$  molecules with an amplitude of approximately 50 fm, which is probed by a time-delayed soft-x-ray pulse at the sulfur  $L_{2,3}$  edge. Mapping the extremely small measured energy shifts to internuclear distances requires an understanding of the electronic contributions provided by a many-body *ab initio* simulation. Our study establishes core-level spectroscopy as a precision tool for time-dependent molecular-structure metrology.

DOI: [10.1103/PhysRevA.108.032816](https://doi.org/10.1103/PhysRevA.108.032816)

Molecular physics and chemistry are governed by electron dynamics but ultimately realized in the structural coordination of the nuclei. The most subtle molecular-structure alterations are vibrations. Hence, exciting and precisely measuring molecular vibrations are crucial for understanding chemical reactions and their control [1–7]. In particular, the interplay between the dynamics of electrons and nuclei is of pivotal interest [4,8–11]. One frontier is the single quantum level by investigating smallest electronic or vibrational [12,13] excitations.

Lasers are a powerful tool for controlling molecular dynamics. In recent decades the electronic population [14], molecular rotation [15], and highly excited vibrational states [16,17] have been successfully targeted by intense light fields. Laser-based infrared (IR) and Raman spectroscopy are well-established techniques in science and industry [18] for investigating electronic and vibrational molecular characteristics in matter. In combination with core-level spectroscopy [19], one gains deep insights into the equilibrium electronic and vibrational structures of molecules and solids [20].

On the other hand, diffraction methods are commonly used to determine the distances and dynamics within matter using, e.g., electrons [21–30], neutrons [31], or photons [32–34].

For gas-phase molecules, these diffraction methods provide nano- to picometer spatial resolutions. Focusing on molecular vibrations, many spectroscopy experiments have revealed dynamics in a time-resolved manner [11,35–41]. So far, the smallest spatially resolved vibrational feature has been measured at 0.6 pm [42]. A quantification of structural changes on the few-femtometer level [43–46] and potentially below [47,48] thus far has been limited to solid-state systems.

In this work we demonstrate time-resolved vibrational metrology of neutral gas-phase molecules with a spatial precision of 14 fm. For a proof-of-principle experiment, we conduct measurements of smallest bond-length changes in sulfur hexafluoride ( $\text{SF}_6$ ) using table-top, time-resolved x-ray-absorption spectroscopy (TRXAS). Here sulfur  $L_{2,3}$ -edge transitions around 173 eV are probed. With this all-optical spectroscopic method, we induce and time resolve coherent vibrational excitations of a molecular ensemble in the perturbative limit.

The general mechanism that enables the tracing of extremely small structural changes with TRXAS is illustrated in Fig. 1(a): Since TRXAS probes the dipole response of the molecular system, the potential-energy curves (PECs) of the involved electronic states are crucial. Incoming soft-x-ray (SXR) radiation induces a dipole transition from the electronic ground-state PEC to an excited state. These two PECs may generally differ in their minimum-energy position ( $d_0$  and  $d_e$ ) as well as in their shape and width. Ultrashort SXR pulses hence can be used to map the internuclear distance  $d$  to the PEC energy difference  $\Delta E$  [see the inset in Fig. 1(a)]. For sufficiently small internuclear changes  $\Delta d$ , this mechanism is general and can be applied independently of the excited-state PEC character. Thus, very small alterations of the electronic ground-state nuclear wave packet can be detected. One widely applicable process to induce such perturbations in the probability-density distribution within the ground-state PEC is nonresonant, impulsive stimulated Raman (ISR) excitation [35,49–51] via an ultrashort IR pulse. Figure 1(b) illustrates how the first vibrationally excited state

\*Present address: Chemical Sciences Division, Lawrence Berkeley National Laboratory, 1 Cyclotron Road, Berkeley, CA 94720, USA; patrick.rupprecht@mpi-hd.mpg.de

†christian.ott@mpi-hd.mpg.de

‡Also at Center for Quantum Dynamics, Ruprecht-Karls-Universität Heidelberg, Im Neuenheimer Feld 226, 69120 Heidelberg, Germany; thomas.pfeifer@mpi-hd.mpg.de

Published by the American Physical Society under the terms of the Creative Commons Attribution 4.0 International license. Further distribution of this work must maintain attribution to the author(s) and the published article's title, journal citation, and DOI. Open access publication funded by the Max Planck Society.

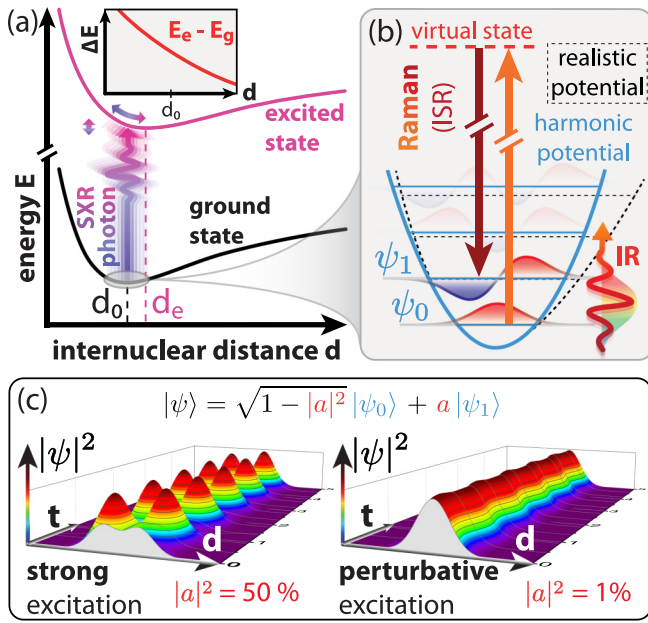


FIG. 1. Mapping vibrational dynamics with core-level spectroscopy. (a) Exemplary PECs of molecular electronic ground and excited states which can be resonantly coupled by SXR radiation. Depending on the internuclear distance  $d$ , the energy differences of the PECs translate into different transition energies  $\Delta E$ , which is illustrated around the equilibrium internuclear distance  $d_0$  in the inset. (b) Vibrational excitation scheme. The ground and first excited nuclear wave functions  $\psi_0$  and  $\psi_1$  of the electronic ground-state PEC are illustrated. A broadband, ultrashort IR pulse can populate the excited state via ISR excitation in a two-photon process. (c) Temporal evolution of the resulting vibrational wave packet  $|\psi(t)|^2$  over five oscillation periods for  $|a|^2 = 50\%$  population (left) of  $|\psi_1\rangle$  and for perturbative excitation ( $|a|^2 = 1\%$ , right).

is coherently populated by coupling it to the ground state in the two-photon ISR process via a virtual state. The ground- and excited-state nuclear wave functions  $\psi_0$  and  $\psi_1$ , with respective energies  $\hbar\omega_0$  and  $\hbar\omega_1$ , can be well approximated by the respective ones from a harmonic potential [52]. The temporal evolution of the vibrational superposition state  $|\psi(t)\rangle = \sqrt{1 - |a|^2}e^{-i\omega_0 t}|\psi_0\rangle + ae^{-i\omega_1 t}|\psi_1\rangle$  after excitation results in a time-dependent probability density  $|\psi(t)|^2$  for different relative populations  $|a|^2$  of the first excited vibrational state  $|\psi_1\rangle$  [see Fig. 1(c)]. While a strong excitation of, e.g.,  $|a|^2 = 50\%$  leads to a quantum-hopping behavior [Fig. 1(c), left], a perturbative excitation [e.g.,  $|a|^2 = 1\%$  in Fig. 1(c), right] approximates an internuclear-distance oscillation of the ground-state-like wave packet. The question arises as to what minimal coherent vibrational excitation and thus bond-length change is measurable within an ensemble of molecules.

To shed light on this extreme perturbative case of coherent molecular excitation, a table-top TRXAS experimental scheme as outlined in Fig. 2 is employed. The optical setup delivers IR laser pulses (center wavelength  $\lambda_c = 1535$  nm) with 1-mJ pulse energy at a 1-kHz repetition rate. The IR pulses are compressed to a three-optical-cycle duration ( $\tau_{\text{FWHM}} = 15$  fs) and temporally characterized with a home-built transient-grating frequency-resolved optical gating apparatus [53]. The

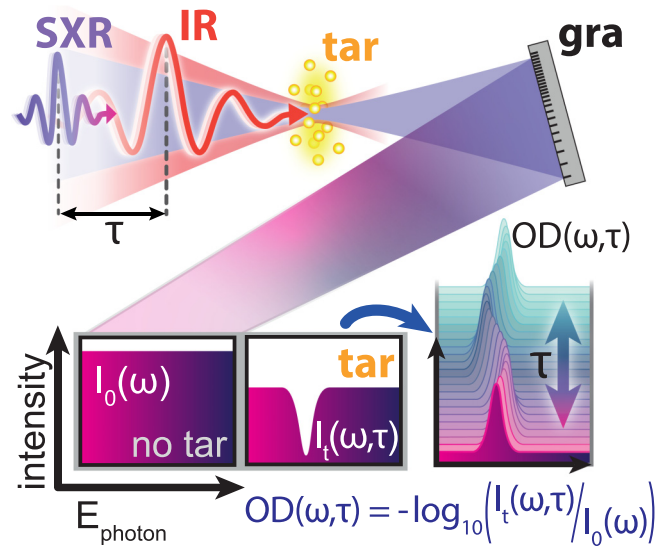


FIG. 2. Experimental TRXAS scheme. Copropagating weak SXR and strong IR pulses are time delayed with respect to each other by  $\tau$ . They are focused into a molecular target (tar), where the preceding IR pulse initiates vibrational dynamics [see Fig. 1(b)] while the SXR pulse probes the system [cf. Fig. 1(a)]. The transmitted SXR pulse is spectrally dispersed by a grating (gra) and measured with an SXR-sensitive CCD camera. Using a reference spectrum without target,  $I_0(\omega)$ , and the transmitted spectra at different times  $\tau$ ,  $I_t(\omega, \tau)$ , a two-dimensional OD( $\omega, \tau$ ) map encodes signatures of electronic and vibrational dynamics.

result of this characterization is plotted as a dark red line in Fig. 4. Focusing these IR pulses into a neon-filled cell inside a vacuum beamline generates SXR photon energies up to 200 eV in a high-order harmonic generation process. Afterward, IR and SXR are spatially separated and time delayed with respect to each other. Finally, the strong IR and comparatively weak SXR beams are refocused into an effusive cell (interaction length of 3 mm) which is filled with 16 mbar of SF<sub>6</sub>. The transmitted SXR spectrum is dispersed by a grating and measured with a CCD camera. Finally, the measured data are evaluated in terms of spectral absorbance [optical density (OD)]. Varying the SXR–IR time delay  $\tau$  results in a time-dependent absorbance OD( $\omega, \tau$ ).

To evaluate the data, we focus on the S  $L_{2,3}$ -edge absorbance doublet  $6a_{1g}$ . This resonance is linked to a dipole transition from the spin-orbit split, core-level S  $2p$  orbital  $2t_{1u}$  ( $j_{\pm} = 3/2, 1/2$ ) to the lowest unoccupied molecular orbital (LUMO)  $6a_{1g}$  [54,55]. The time-delay-dependent resonant absorbance spectra for an IR intensity of  $I_{\text{IR},1} = 9$  TW/cm<sup>2</sup> are shown in Fig. 3(a). In order to gather enough statistics for extracting smallest vibrational signatures, the total uninterrupted measurement duration for this data set is 16 h. An example of a single measured  $2t_{1u} \rightarrow 6a_{1g}$  doublet absorbance is given in Fig. 3(b). To extract small time-dependent signatures, a mean over SXR-first spectra is subtracted from all OD( $\tau$ ) absorbances. The resulting  $\Delta OD(\omega, \tau)$  in Fig. 3(c) shows an oscillatory behavior in the IR-first region ( $\tau > 0$  fs). For quantification purposes, a Voigt model is fitted to the OD( $\omega, \tau$ ) data from Fig. 3(a). Further details on the fitting procedure are given in [56]. A comparison

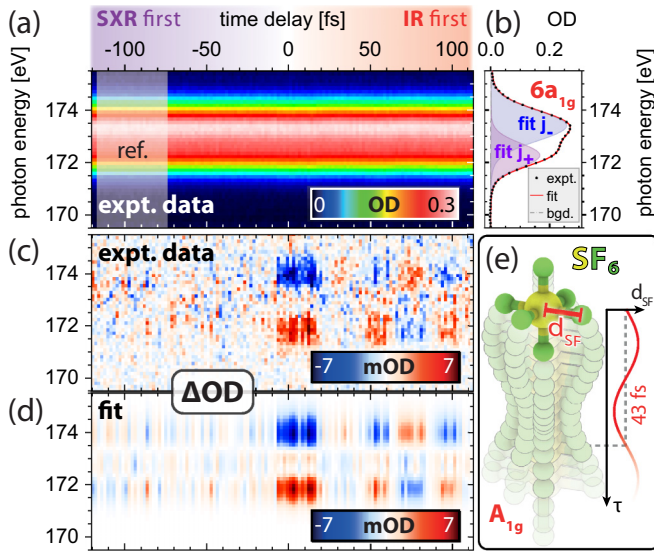


FIG. 3. TRXAS data at the sulfur  $L_{2,3}$  edge in  $\text{SF}_6$ . (a) Measured absorbance  $\text{OD}(\omega, \tau)$  at an IR intensity of  $9 \text{ TW}/\text{cm}^2$ . (b) Spectral lineout from (a) showing the  $6a_{1g}$  doublet resonance as well as its fit and the background (bgd.) of nonresonant absorption into the ionization continuum. (c) Experimental differential absorbance data  $\Delta\text{OD}(\omega, \tau)$  calculated from (a) by subtracting the indicated reference mean spectrum [ref. in (a)]. (d)  $\Delta\text{OD}(\omega, \tau)$  based on the fits of the data in (a). (e) Illustration of the symmetric vibrational breathing mode  $A_{1g}$  in  $\text{SF}_6$  which has the same period as the oscillatory signature visible in (c) or (d) for  $\tau > 50 \text{ fs}$ .

of the experimental  $\Delta\text{OD}$  [Fig. 3(c)] and the  $\Delta\text{OD}$  based on the fits [Fig. 3(d)] verifies that the measured time-dependent features are reproduced by the fits. The periodicity of the oscillatory signatures out of pulse overlap ( $\tau > 50 \text{ fs}$ ) in the data coincides with the symmetric breathing mode vibration  $A_{1g}$  of  $\text{SF}_6$  with a 43-fs period [35,57]. Such a vibration is visualized in Fig. 3(e). In addition, a second measurement was conducted with a higher IR intensity of  $I_{\text{IR},2} = 26 \text{ TW}/\text{cm}^2$  which allows us to investigate the IR-intensity dependence of the involved electronic and vibrational dynamics. To summarize the fit results of both data sets, Fig. 4 shows the resonance energy shift  $\Delta E_c$  for both doublet peaks  $6a_{1g}(j_{\pm})$  and both intensities  $I_{\text{IR},1/2}$  matched to each other (right ordinate axis for the  $I_{\text{IR},2}$  data set). Here  $\Delta E_c$  refers to the shifts in measured transition energy from the many-body ground state to the  $2t_{1u}^{-1}6a_{1g}^1(j_{\pm})$  core-level excited state doublet. These shifts are sensitive to both purely electronic dynamics in temporal pulse overlap and the molecular vibrational dynamics.

In order to gain further insight into the oscillatory behavior of the  $6a_{1g}$  peak energies for the IR-first case, a quantum-mechanical *ab initio* simulation is combined with a classical force approach for the  $9\text{-TW}/\text{cm}^2$  data set. First, the contributing orbitals are calculated using the density-functional theory (DFT) full-potential local-orbital (FPLO) code [58,59] for different  $d_{\text{SF}}$  internuclear distances. Second, the impact of the IR pulse is included in a quantum-mechanical many-body restricted active-space simulation [60] by off-resonant dipole coupling of the highest occupied molecular orbital and the LUMO. The corresponding Hamiltonian is used for the temporal propagation of the electronic wave function of the

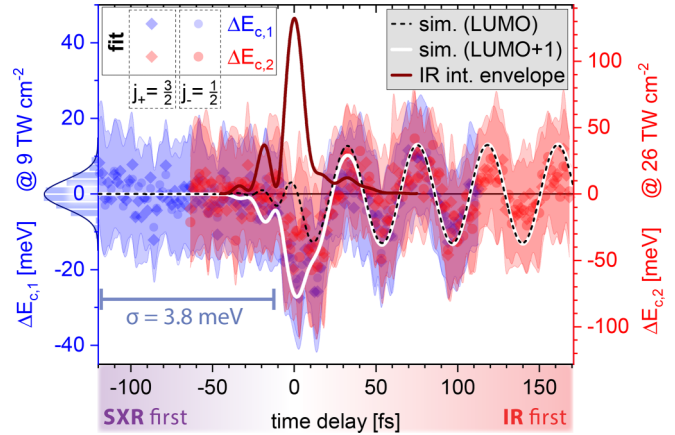


FIG. 4. Temporal evolution of  $6a_{1g}$  resonance energy shifts. Resonance energy differences  $\Delta E_c$  [with respect to ref. in Fig. 3(a)] extracted from the Voigt fits of the TRXAS experimental data in Fig. 3 over the SXR-IR time delay. Two measurements with different IR intensities are shown (blue for  $9 \text{ TW}/\text{cm}^2$  and red for  $26 \text{ TW}/\text{cm}^2$ , left and right ordinate axes, respectively). For each measurement, the  $6a_{1g}(j_+)$  and  $6a_{1g}(j_-)$  absorbance-peak energy differences are indicated as diamonds and circles, respectively, including the fit uncertainties. Simulation results without (black dashed line) and with (white solid line) taking the first LUMO + 1 orbital with ungerade symmetry ( $6t_{1u}$ ) into account. A standard deviation of  $\sigma = 3.8 \text{ meV}$  for the SXR-first region of  $\Delta E_{c,1}$  (blue histogram) is determined. Furthermore, the measured IR pulse intensity envelope is illustrated (dark red line).

system via the time-dependent Schrödinger equation. This results in a laser-dressed ground-state PEC and hence in a slightly changed equilibrium internuclear distance  $d_0$ . Consequently, the nuclei are accelerated classically according to the laser-dressed PEC's slope and result in a new molecular structure after a time step  $\delta t$ . The simulation utilizes the Born-Oppenheimer approximation, where the electronic structure follows the nuclear redistribution immediately. Thus, the DFT orbitals of the updated molecular structure are used as input for the next time step. For each time step, the resulting  $6a_{1g}$  absorbance of the SXR probe pulse is calculated with the QUANTY code [61,62], which results in the black dashed line in Fig. 4. The agreement within the SXR-IR temporal pulse overlap is further improved (white solid line) by calculating Stark shifts of the effective LUMO through its dipole coupling to the first unoccupied molecular orbital (LUMO + 1) with ungerade symmetry ( $6t_{1u}$ ) via the measured IR intensity envelope (dark red line). Here, including higher-excited LUMO +  $n$  (with  $n > 1$ ) DFT-based molecular orbitals does not lead to a significant change within the signal-to-noise ratio of the experiment due to the far-off-resonant nature of the respective dipole couplings.

The transient energy shift during time overlap is due to an electronic ac Stark effect [63], which is proportional to the IR intensity. For time delays greater than 50 fs, the observed energy shifts are purely caused by vibrational dynamics. Here the ISR excitation leads to an S-F excursion amplitude which scales linearly with the IR intensity [64,65]. Due to the perturbative excitation, the impact of the bond-length change on the resonance energy shift can be approximated to be linear.



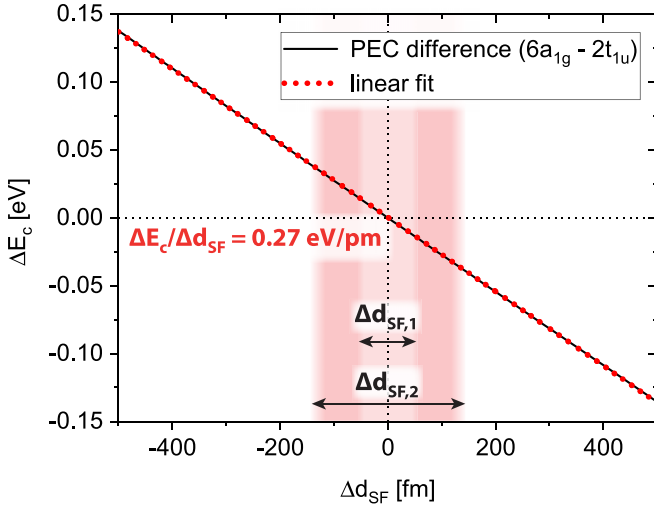


FIG. 5. Mapping of transition energy shift of  $6a_{1g}$  doublet to S-F bond-length change in  $\text{SF}_6$ . The transition-energy shift calculated via the PEC difference of ground and  $6a_{1g}$  excited states is depicted as the black solid line. Additionally, the linear fit resulting in a slope value of  $\frac{\Delta E_c}{\Delta d_{\text{SF}}} = 0.27$  eV/pm is shown as a red dashed line and the regions of interest for the 9 TW/cm<sup>2</sup> ( $\Delta d_{\text{SF},1}$ ) and the 26 TW/cm<sup>2</sup> ( $\Delta d_{\text{SF},2}$ ) experiment. No noticeable difference to the fit is observed, which illustrates the validity of the linear fit.

Hence, the overall energy shift  $\Delta E_c(t)$  originating from the combined electronic and vibrational dynamics is also proportional to the IR intensity and enables us to match the two data sets  $\Delta E_{c,1}$  and  $\Delta E_{c,2}$  in Fig. 4 by simply rescaling the ordinate axis by their intensity ratio  $I_{\text{IR},1}/I_{\text{IR},2}$ .

To elucidate the perturbative limit of vibrational excitation, the low-IR-intensity ( $I_{\text{IR},1} = 9$  TW/cm<sup>2</sup>) data set  $\Delta E_{c,1}$  is analyzed in more detail: For vibrational metrology with TRXAS, the transition-energy shift with respect to the bond-length change is crucial [compare Fig. 1(a) inset]. With

the calculated electronic many-body ground-state and the many-body excited-state  $2t_{1u}^{-1}6a_{1g}$  PECs of  $\text{SF}_6$ , a linear slope value of  $\frac{\Delta E_c}{\Delta d_{\text{SF}}} = 0.27$  eV/pm around the ground-state equilibrium S-F distance  $d_0 = 1.561$  Å [66] is determined as shown in Fig. 5. This slope value is in good agreement with the recent results by Barreau *et al.* [67] indicating  $\frac{\Delta E_c}{\Delta d_{\text{SF}}} = 0.29$  eV/pm. Figure 6(a) illustrates the symmetric  $A_{1g}$  vibration around  $d_0$  for a single S-F bond. This vibration is governed by the electronic ground-state PEC of the Raman-active  $A_{1g}$  vibrations shown in Fig. 6(b). For large vibrational excitations this PEC describes a dissociation to  $\text{S} + 6\text{F}$  with a dissociation energy of 22.4 eV [68]. Due to the perturbative vibrational excitation, only a small region of the PEC around  $d_0$  is relevant as illustrated in Fig. 6(c). The vibrational frequency  $\nu_{A_{1g}} = 775$  cm<sup>-1</sup> [57] of the first excited breathing mode  $A_{1g}$  in  $\text{SF}_6$  is equivalent to a vibrational energy-level spacing of 96 meV. While two further Raman active modes ( $\nu_2 = 642$  cm<sup>-1</sup> and  $\nu_5 = 525$  cm<sup>-1</sup>) exist, they are much weaker than the fundamental breathing mode  $A_{1g}$  [35] and hence are not observed in this perturbative vibrational excitation experiment. Furthermore, Fig. 6(c) shows the probability densities of the ground- and first-excited-state nuclear wave functions  $|\psi_0\rangle$  and  $|\psi_1\rangle$  [compare Fig. 1(b)], respectively, for the case of  $A_{1g}$  vibrations in  $\text{SF}_6$ . The thermal excitation at room temperature (300 K) leads to a population of the first excited  $A_{1g}$  vibrational state of  $|a|^2 = 2.4\%$ . In the lower half of Fig. 6(c), the 100-time-magnified view of the thermally excited probability density (in orange) is compared to the one of the vibrational ground state (in blue). In contrast, the ISR excitation with a 9-TW/cm<sup>2</sup>-intensity IR pulse leads to an excited-state population of  $|a|^2 < 0.04\%$ , which is illustrated with a magnification of 1000 (in red) in the upper half of Fig. 6(c). Notably, this is a 60-time-smaller vibrational excitation compared to the thermally induced population. Due to the coherent nature of ISR excitation, however, the excitation in the perturbative limit can be well separated from the incoherent thermal vibrational background. The small deviations from the stepwise behavior

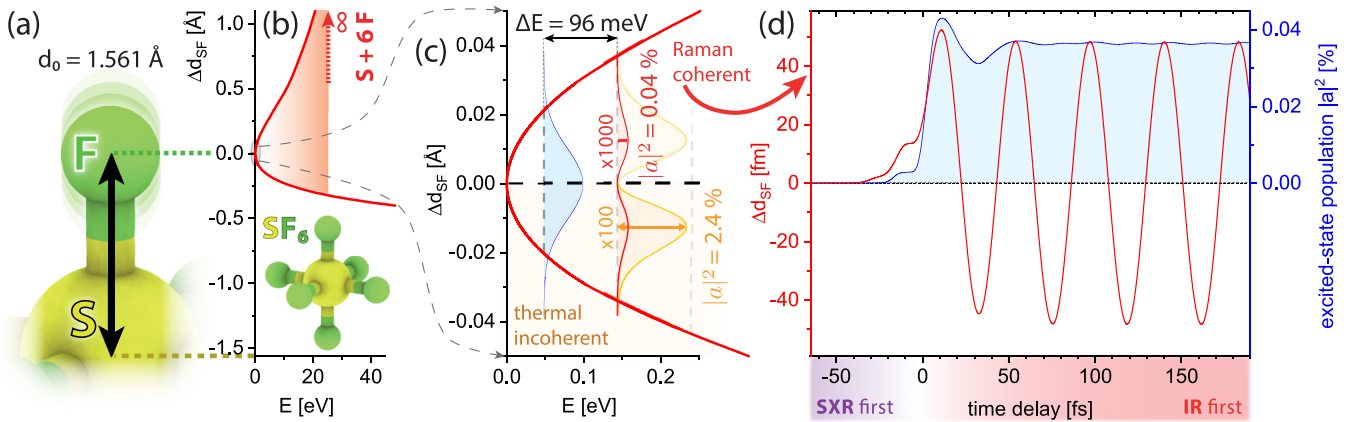


FIG. 6. Femtometer-resolved, perturbatively excited vibration in  $\text{SF}_6$ . (a) Illustration of a single S-F bond in  $\text{SF}_6$  [full molecular structure in (b)] vibrating around the equilibrium distance  $d_0$ . (b) Calculated electronic ground-state PEC of symmetric breathing mode  $A_{1g}$  vibrations in  $\text{SF}_6$ . (c) Close-up of (b) around  $d_0$  with illustrations of the probability density of the vibrational ground state (blue) and the first excited state  $A_{1g}$  (red or orange). A comparison is given for the population of  $A_{1g}$  due to incoherent thermal excitation at 300 K (orange) and the 60 times smaller measured coherent ISR excitation (red) by the  $I_{\text{IR},1} = 9$  TW/cm<sup>2</sup> IR pulse. (d) Calculated bond-length difference  $\Delta d_{\text{SF}}$  and population of  $A_{1g}$ ,  $|a|^2$ , over SXR-IR time delay.

of the population dynamics in Fig. 6(d) (blue line) are linked to the temporal IR pulse structure. As a result, a vibrational amplitude of  $\Delta d_{\text{SF}} \approx 50$  fm [compare Fig. 6(d), red line] is extracted from the simulation. From the  $\sigma = 3.8$  meV standard deviation of the  $\Delta E_{c,1}$  data set in Fig. 4 within the SXR-first region, a precision of 14 fm is determined. This equals around two times the 6.5-fm core diameter of the sulfur atom [69] and translates into a relative bond-length-change sensitivity of  $10^{-4}$ . With a systematic deviation of less than 10% between the PEC-slope values of Barreau *et al.* [67] and our calculation, the corresponding systematic uncertainty of less than 5 fm for the retrieved 50-fm oscillation amplitude is well below the statistical 14-fm precision.

Overall, our approach for perturbative vibrational control is very general: The widely applicable ISR excitation scheme is easily scalable. Even the smallest induced coherent vibrational amplitudes can be separated from the thermal incoherent background and no special preparation of the gas-phase target (e.g., orientation or alignment) is needed. In addition, due to its perturbative nature acting on neutral molecules, the presented technique is potentially of interest for real-time precision observation and control of chemical reactions. Moreover, our study reveals the technical potential of using an all-optical table-top method for precision metrology of time-dependent molecular dynamics, which complements techniques that determine absolute molecular structure like x-ray [32–34] or ultrafast electron diffraction [21–24]. In the future, high-accuracy perturbative quantum control in neutral gas-phase molecules is in reach using TRXAS. This is espe-

cially of interest for vibrational and rotational ground-state chemistry in cryogenic environments, e.g., astrochemistry [70]. Furthermore, vibrational precision control might be a suitable tool to accurately manipulate nonadiabatic dynamics very close to conical intersections, which are crucial for photochemistry [71]. As the perturbative excitation of a molecular ensemble is measured, there is no fundamental physical restriction concerning exciting and measuring even smaller vibrational amplitudes. Hence, using a high-resolution SXR spectrometer [72–74] and a high-repetition-rate laser system [75,76] to increase statistics, a subfemtometer precision seems feasible in the future. These results thus substantially advance the field of x-ray spectroscopy in molecules [77–79] by paving the way for time-resolved vibrational precision metrology.

We thank C. Kaiser and his team for technical support. We acknowledge financial support from the Deutsche Forschungsgemeinschaft (DFG) (German Research Foundation) under Germany's Excellence Strategy EXC2181/1-390900948 (the Heidelberg STRUCTURES Excellence Cluster) and from the European Research Council (Grant No. X-MuSiC 616783). Furthermore, we acknowledge support from the state of Baden-Württemberg through bwHPC and the DFG through Grant No. INST 40/575-1 FUGG (JUSTUS 2 cluster). P.R. acknowledges funding from the Alexander von Humboldt Foundation (Feodor Lynen Fellowship).

- [1] A. Zavriyev, P. H. Bucksbaum, J. Squier, and F. Saline, Light-Induced Vibrational Structure in  $\text{H}_2^+$  and  $\text{D}_2^+$  in Intense Laser Fields, *Phys. Rev. Lett.* **70**, 1077 (1993).
- [2] F. F. Crim, Bond-selected chemistry: Vibrational state control of photodissociation and bimolecular reaction, *J. Phys. Chem.* **100**, 12725 (1996).
- [3] V. S. Letokhov, Use of lasers to control selective chemical reactions, *Science* **180**, 451 (1973).
- [4] L. S. Cederbaum, The multistate vibronic coupling problem, *J. Chem. Phys.* **78**, 5714 (1983).
- [5] A. H. Zewail, Femtochemistry: Atomic-scale dynamics of the chemical bond, *J. Phys. Chem. A* **104**, 5660 (2000).
- [6] T. C. Weinacht, R. Bartels, S. Backus, P. H. Bucksbaum, B. Pearson, J. M. Geremia, H. Rabitz, H. C. Kapteyn, and M. M. Murnane, Coherent learning control of vibrational motion in room temperature molecular gases, *Chem. Phys. Lett.* **344**, 333 (2001).
- [7] J. Neugebauer, E. J. Baerends, and M. Nooijen, Vibronic coupling and double excitations in linear response time-dependent density functional calculations: Dipole-allowed states of  $\text{N}_2$ , *J. Chem. Phys.* **121**, 6155 (2004).
- [8] R. L. Fulton and M. Gouterman, Vibronic coupling. I. Mathematical treatment for two electronic states, *J. Chem. Phys.* **35**, 1059 (1961).
- [9] G. A. Worth and L. S. Cederbaum, Beyond Born-Oppenheimer: Molecular dynamics through a conical intersection, *Annu. Rev. Phys. Chem.* **55**, 127 (2004).
- [10] Y. Kobayashi, K. F. Chang, T. Zeng, D. M. Neumark, and S. R. Leone, Direct mapping of curve-crossing dynamics in IBr by attosecond transient absorption spectroscopy, *Science* **365**, 79 (2019).
- [11] K. S. Zinchenko, F. Ardana-Lamas, I. Seidu, S. P. Neville, J. van der Veen, V. U. Lanfaloni, M. S. Schuurman, and H. J. Wörner, Sub-7-femtosecond conical-intersection dynamics probed at the carbon K-edge, *Science* **371**, 489 (2021).
- [12] G. Cerchiari, G. Araneda, L. Podhora, L. Slodička, Y. Colombe, and R. Blatt, Measuring Ion Oscillations at the Quantum Level with Fluorescence Light, *Phys. Rev. Lett.* **127**, 063603 (2021).
- [13] S. T. Velez, K. Seibold, N. Kipfer, M. D. Anderson, V. Sudhir, and C. Galland, Preparation and Decay of a Single Quantum of Vibration at Ambient Conditions, *Phys. Rev. X* **9**, 041007 (2019).
- [14] N. V. Vitanov, A. A. Rangelov, B. W. Shore, and K. Bergmann, Stimulated Raman adiabatic passage in physics, chemistry, and beyond, *Rev. Mod. Phys.* **89**, 015006 (2017).
- [15] E. T. Karamatskos, S. Raabe, T. Mullins, A. Trabatonni, P. Stammer, G. Goldsztejn, R. R. Johansen, K. Długołęcki, H. Stapelfeldt, M. J. Vrakking, S. Trippel, A. Rouzée, and J. Küpper, Molecular movie of ultrafast coherent rotational dynamics of OCS, *Nat. Commun.* **10**, 3364 (2019).
- [16] T. Baumert, M. Grosser, R. Thalweiser, and G. Gerber, Femtosecond Time-Resolved Molecular Multiphoton Ionization: The  $\text{Na}_2$  System, *Phys. Rev. Lett.* **67**, 3753 (1991).

- [17] P. Wustelt, F. Oppermann, S. Mhatre, M. Kübel, A. M. Saylor, M. Lein, S. Gräfe, and G. G. Paulus, Laser-Driven Anharmonic Oscillator: Ground-State Dissociation of the Helium Hydride Molecular Ion by Midinfrared Pulses, *Phys. Rev. Lett.* **127**, 043202 (2021).
- [18] I. R. Lewis and H. Edwards, *Handbook of Raman spectroscopy: From the Research Laboratory to the Process Line* (CRC, Boca Raton, 2001).
- [19] K. Siegbahn, Electron spectroscopy for atoms, molecules, and condensed matter, *Science* **217**, 111 (1982).
- [20] L. J. P. Ament, M. van Veenendaal, T. P. Devereaux, J. P. Hill, and J. van den Brink, Resonant inelastic x-ray scattering studies of elementary excitations, *Rev. Mod. Phys.* **83**, 705 (2011).
- [21] G. Sciaini and R. J. D. Miller, Femtosecond electron diffraction: Heralding the era of atomically resolved dynamics, *Rep. Prog. Phys.* **74**, 096101 (2011).
- [22] X. Shen, J. P. F. Nunes, J. Yang, R. K. Jobe, R. K. Li, M.-F. Lin, B. Moore, M. Niebuhr, S. Weathersby, T. J. A. Wolf, C. Yoneda, M. Guehr, M. Centurion, and X. J. Wang, Femtosecond gas-phase mega-electron-volt ultrafast electron diffraction, *Struct. Dyn.* **6**, 054305 (2019).
- [23] J. Yang, M. Guehr, X. Shen, R. Li, T. Vecchione, R. Coffee, J. Corbett, A. Fry, N. Hartmann, C. Hast, K. Hegazy, K. Jobe, I. Makasyuk, J. Robinson, M. S. Robinson *et al.*, Diffractive Imaging of Coherent Nuclear Motion in Isolated Molecules, *Phys. Rev. Lett.* **117**, 153002 (2016).
- [24] E. G. Champenois, D. M. Sanchez, J. Yang, J. P. Figueira Nunes, A. Attar, M. Centurion, R. Forbes, M. Gühr, K. Hegazy, F. Ji, S. K. Saha, Y. Liu, M.-F. Lin, D. Luo, B. Moore *et al.*, Conformer-specific photochemistry imaged in real space and time, *Science* **374**, 178 (2021).
- [25] A. H. Zewail, Four-dimensional electron microscopy, *Science* **328**, 187 (2010).
- [26] C. I. Blaga, J. Xu, A. D. DiChiara, E. Sistrunk, K. Zhang, P. Agostini, T. A. Miller, L. F. DiMauro, and C. Lin, Imaging ultrafast molecular dynamics with laser-induced electron diffraction, *Nature (London)* **483**, 194 (2012).
- [27] B. Wolter, M. G. Pullen, A.-T. Le, M. Baudisch, K. Doblhoff-Dier, A. Senftleben, M. Hemmer, C. D. Schröter, J. Ullrich, T. Pfeifer, R. Moshhammer, S. Gräfe, O. Vendrell, C. D. Lin, and J. Biegert, Ultrafast electron diffraction imaging of bond breaking in di-ionized acetylene, *Science* **354**, 308 (2016).
- [28] A. Sanchez, K. Amini, S.-J. Wang, T. Steinle, B. Belsa, J. Danek, A.-T. Le, X. Liu, R. Moshhammer, T. Pfeifer, M. Richter, J. Ullrich, S. Gräfe, C. D. Lin, and J. Biegert, Molecular structure retrieval directly from laboratory-frame photoelectron spectra in laser-induced electron diffraction, *Nat. Commun.* **12**, 1520 (2021).
- [29] R. Puthumpally-Joseph, J. Viau-Trudel, M. Peters, T. T. Nguyen-Dang, O. Atabek, and E. Charron, Inversion of strong-field photoelectron spectra for molecular orbital imaging, *Phys. Rev. A* **94**, 023421 (2016).
- [30] R. Puthumpally-Joseph, J. Viau-Trudel, M. Peters, T. Nguyen-Dang, O. Atabek, and E. Charron, Laser-induced electron diffraction: Inversion of photo-electron spectra for molecular orbital imaging, *Mol. Phys.* **115**, 1889 (2017).
- [31] B. Jacrot, The study of biological structures by neutron scattering from solution, *Rep. Prog. Phys.* **39**, 911 (1976).
- [32] B. E. Warren, *X-Ray Diffraction* (Courier, Chelmsford, 1990).
- [33] J. Küpper, S. Stern, L. Holmegaard, F. Filsinger, A. Rouzée, A. Rudenko, P. Johnsson, A. V. Martin, M. Adolph, A. Aquila, S. Bajt, A. Barty, C. Bostedt, J. Bozek, C. Caleman *et al.*, X-Ray Diffraction from Isolated and Strongly Aligned Gas-Phase Molecules with a Free-Electron Laser, *Phys. Rev. Lett.* **112**, 083002 (2014).
- [34] B. Stankus, H. Yong, N. Zotev, J. M. Ruddock, D. Bellshaw, T. J. Lane, M. Liang, S. Boutet, S. Carbajo, J. S. Robinson *et al.*, Ultrafast x-ray scattering reveals vibrational coherence following Rydberg excitation, *Nat. Chem.* **11**, 716 (2019).
- [35] N. L. Wagner, A. Wüest, I. P. Christov, T. Popmintchev, X. Zhou, M. M. Murnane, and H. C. Kapteyn, Monitoring molecular dynamics using coherent electrons from high harmonic generation, *Proc. Natl. Acad. Sci. USA* **103**, 13279 (2006).
- [36] K. Kunnus, M. Vacher, T. C. B. Harlang, K. S. Kjær, K. Haldrup, E. Biasin, T. B. van Driel, M. Pápai, P. Chabera, Y. Liu, H. Tatsuono, C. Timm, E. Källman, M. Delcey, R. W. Hartsocock *et al.*, Vibrational wavepacket dynamics in Fe carbene photosensitizer determined with femtosecond x-ray emission and scattering, *Nat. Commun.* **11**, 634 (2020).
- [37] E. R. Hosler and S. R. Leone, Characterization of vibrational wave packets by core-level high-harmonic transient absorption spectroscopy, *Phys. Rev. A* **88**, 023420 (2013).
- [38] H. Timmers, X. Zhu, Z. Li, Y. Kobayashi, M. Sabbar, M. Hollstein, M. Reduzzi, T. J. Martínez, D. M. Neumark, and S. R. Leone, Disentangling conical intersection and coherent molecular dynamics in methyl bromide with attosecond transient absorption spectroscopy, *Nat. Commun.* **10**, 3133 (2019).
- [39] Y. Kobayashi, K. F. Chang, S. M. Poullain, V. Scutelnic, T. Zeng, D. M. Neumark, and S. R. Leone, Coherent electronic-vibrational dynamics in deuterium bromide probed via attosecond transient-absorption spectroscopy, *Phys. Rev. A* **101**, 063414 (2020).
- [40] N. Saito, H. Sannohe, N. Ishii, T. Kanai, N. Kosugi, Y. Wu, A. Chew, S. Han, Z. Chang, and J. Itatani, Real-time observation of electronic, vibrational, and rotational dynamics in nitric oxide with attosecond soft x-ray pulses at 400 eV, *Optica* **6**, 1542 (2019).
- [41] Y. Pertot, C. Schmidt, M. Matthews, A. Chauvet, M. Huppert, V. Svoboda, A. von Conta, A. Tehlar, D. Baykusheva, J.-P. Wolf, and H. J. Wörner, Time-resolved x-ray absorption spectroscopy with a water window high-harmonic source, *Science* **355**, 264 (2017).
- [42] Z. Wei, J. Li, L. Wang, S. T. See, M. H. Jhon, Y. Zhang, F. Shi, M. Yang, and Z.-H. Loh, Elucidating the origins of multimode vibrational coherences of polyatomic molecules induced by intense laser fields, *Nat. Commun.* **8**, 735 (2017).
- [43] R. F. Pettifer, O. Mathon, S. Pascarelli, M. D. Cooke, and M. R. J. Gibbs, Measurement of femtometre-scale atomic displacements by x-ray absorption spectroscopy, *Nature (London)* **435**, 78 (2005).
- [44] J. Weisshaupt, A. Rouzée, M. Woerner, M. J. J. Vrakking, T. Elsaesser, E. L. Shirley, and A. Borgschulte, Ultrafast modulation of electronic structure by coherent phonon excitations, *Phys. Rev. B* **95**, 081101(R) (2017).
- [45] W. Jo, E. C. Landahl, A. D. DiChiara, D. A. Walko, and S. Lee, Measuring femtometer lattice displacements driven by free carrier diffusion in a polycrystalline semiconductor using time-resolved x-ray scattering, *Appl. Phys. Lett.* **113**, 032107 (2018).

- [46] B. K. De, V. Dwij, R. Misawa, T. Kimura, and V. G. Sathe, Femtometer atomic displacement, the root cause for multiferroic behavior of CuO unearthed through polarized Raman spectroscopy, *J. Phys.: Condens. Matter* **33**, 12LT01 (2021).
- [47] M. Kozina, T. Hu, J. Wittenberg, E. Szilagy, M. Trigo, T. Miller, C. Uher, A. Damodaran, L. Martin, A. Mehta, J. Corbett, J. Safranek, D. A. Reis, and A. M. Lindenberg, Measurement of transient atomic displacements in thin films with picosecond and femtometer resolution, *Struct. Dyn.* **1**, 034301 (2014).
- [48] Z. Wu, L. Zhang, M. Zhang, I. L. Li, H. Su, H. Zhao, S. Ruan, and H. Liang, Graphene plasmon resonances for electrically-tunable sub-femtometer dimensional resolution, *Nanomaterials* **10**, 1381 (2020).
- [49] A. M. Walsh and R. F. Loring, Theory of resonant and nonresonant impulsive stimulated Raman scattering, *Chem. Phys. Lett.* **160**, 299 (1989).
- [50] A. M. Weiner, D. E. Leaird, G. P. Wiederrecht, and K. A. Nelson, Femtosecond pulse sequences used for optical manipulation of molecular motion, *Science* **247**, 1317 (1990).
- [51] M. Wittmann, A. Nazarkin, and G. Korn, fs-Pulse Synthesis Using Phase Modulation by Impulsively Excited Molecular Vibrations, *Phys. Rev. Lett.* **84**, 5508 (2000).
- [52] E. B. Wilson, J. C. Decius, and P. C. Cross, *Molecular Vibrations: The Theory of Infrared and Raman Vibrational Spectra* (Courier, Chelmsford, 1980).
- [53] P. Rupprecht, A. Magunia, L. Aufleger, C. Ott, and T. Pfeifer, Flexible experimental platform for dispersion-free temporal characterization of ultrashort pulses, [arXiv:2308.14858](https://arxiv.org/abs/2308.14858).
- [54] E. Hudson, D. A. Shirley, M. Domke, G. Remmers, A. Puschmann, T. Mandel, C. Xue, and G. Kaindl, High-resolution measurements of near-edge resonances in the core-level photoionization spectra of SF<sub>6</sub>, *Phys. Rev. A* **47**, 361 (1993).
- [55] J. L. Dehmer, Evidence of effective potential barriers in the x-ray absorption spectra of molecules, *J. Chem. Phys.* **56**, 4496 (1972).
- [56] P. Rupprecht, L. Aufleger, S. Heinze, A. Magunia, T. Ding, M. Rebholz, S. Amberg, N. Mollov, F. Henrich, M. W. Haverkort *et al.*, Laser Control of Electronic Exchange Interaction within a Molecule, *Phys. Rev. Lett.* **128**, 153001 (2022).
- [57] A. Aboumajd, H. Berger, and R. Saint-Loup, Analysis of the Raman spectrum of SF<sub>6</sub>, *J. Mol. Spectrosc.* **78**, 486 (1979).
- [58] K. Koepernik and H. Eschrig, Full-potential nonorthogonal local-orbital minimum-basis band-structure scheme, *Phys. Rev. B* **59**, 1743 (1999).
- [59] K. Koepernik *et al.*, FPLO website, <https://www.fplo.de> (2023).
- [60] R. V. Pinjari, M. G. Delcey, M. Guo, M. Odelius, and M. Lundberg, Restricted active space calculations of L-edge x-ray absorption spectra: From molecular orbitals to multiplet states, *J. Chem. Phys.* **141**, 124116 (2014).
- [61] M. W. Haverkort, M. Zwierzycki, and O. K. Andersen, Multiplet ligand-field theory using Wannier orbitals, *Phys. Rev. B* **85**, 165113 (2012).
- [62] M. W. Haverkort *et al.*, Quany website, <http://www.quany.org> (2023).
- [63] J. S. Bakos, AC Stark effect and multiphoton processes in atoms, *Phys. Rep.* **31**, 209 (1977).
- [64] R. A. Bartels, S. Backus, M. M. Murnane, and H. C. Kapteyn, Impulsive stimulated Raman scattering of molecular vibrations using nonlinear pulse shaping, *Chem. Phys. Lett.* **374**, 326 (2003).
- [65] Y. R. Shen and N. Bloembergen, Theory of stimulated Brillouin and Raman scattering, *Phys. Rev.* **137**, A1787 (1965).
- [66] L. S. Bartell and S. K. Doun, Structures of hexacoordinate compounds of main-group elements: Part III. An electron diffraction study of SF<sub>6</sub>, *J. Mol. Struct.* **43**, 245 (1978).
- [67] L. Barreau, A. D. Ross, V. Kimberg, P. Krasnov, S. Blinov, D. M. Neumark, and S. R. Leone, Core-excited states of SF<sub>6</sub> probed with soft-x-ray femtosecond transient absorption of vibrational wave packets, *Phys. Rev. A* **108**, 012805 (2023).
- [68] V. H. Dibeler and F. Mohler, Dissociation of SF<sub>6</sub>, CF<sub>4</sub>, and SiF<sub>4</sub> by electron impact, *J. Res. Natl. Bur. Stand.* **40**, 25 (1948).
- [69] L. A. Schaller, D. A. Barandao, P. Bergem, M. Boschung, T. Q. Phan, G. Piller, A. Rüttschi, L. Schellenberg, H. Schneuwly, G. Fricke, G. Mallot, and H. G. Sieberling, Nuclear charge radii of the even sulphur isotopes <sup>32</sup>S, <sup>34</sup>S, and <sup>36</sup>S and of <sup>31</sup>P using muonic atoms, *Phys. Rev. C* **31**, 1007 (1985).
- [70] K. I. Öberg, Photochemistry and astrochemistry: Photochemical pathways to interstellar complex organic molecules, *Chem. Rev.* **116**, 9631 (2016).
- [71] M. S. Schuurman and A. Stolow, Dynamics at conical intersections, *Annu. Rev. Phys. Chem.* **69**, 427 (2018).
- [72] C. Kleine, M. Ekimova, M.-O. Winhart, S. Eckert, O. Reichel, H. Löchel, J. Probst, C. Braig, C. Seifert, A. Erko, A. Sokolov, M. J. J. Vrakking, E. T. J. Nibbering, and A. Rouzée, Highly efficient soft x-ray spectrometer for transient absorption spectroscopy with broadband table-top high harmonic sources, *Struct. Dyn.* **8**, 034302 (2021).
- [73] S. G. Chiuzbăian, C. F. Hague, A. Avila, R. Delaunay, N. Jaouen, M. Sacchi, F. Polack, M. Thomasset, B. Lagarde, A. Nicolaou, S. Brignolo, C. Baumier, J. Lüning, and J.-M. Mariot, Design and performance of AERHA, a high acceptance high resolution soft x-ray spectrometer, *Rev. Sci. Instrum.* **85**, 043108 (2014).
- [74] Y. Harada, M. Kobayashi, H. Niwa, Y. Senba, H. Ohashi, T. Tokushima, Y. Horikawa, S. Shin, and M. Oshima, Ultrahigh resolution soft x-ray emission spectrometer at BL07LSU in SPring-8, *Rev. Sci. Instrum.* **83**, 013116 (2012).
- [75] P.-A. Chevreuil, F. Brunner, S. Hrisafov, J. Pupekis, C. R. Phillips, U. Keller, and L. Gallmann, Water-window high harmonic generation with 0.8- $\mu$ m and 2.2- $\mu$ m OPCPAs at 100 kHz, *Opt. Express* **29**, 32996 (2021).
- [76] T. Witting, M. Osolodkov, F. Schell, F. Morales, S. Patchkovskii, P. Šušnjar, F. H. Cavalcante, C. S. Menoni, C. P. Schulz, F. J. Furch *et al.*, Generation and characterization of isolated attosecond pulses at 100 kHz repetition rate, *Optica* **9**, 145 (2022).
- [77] R. Geneaux, H. J. B. Marroux, A. Guggenmos, D. M. Neumark, and S. R. Leone, Transient absorption spectroscopy using high harmonic generation: A review of ultrafast x-ray dynamics in molecules and solids, *Philos. Trans. R. Soc. A* **377**, 20170463 (2019).
- [78] P. M. Kraus, M. Zürich, S. K. Cushing, D. M. Neumark, and S. R. Leone, The ultrafast x-ray spectroscopic revolution in chemical dynamics, *Nat. Rev. Chem.* **2**, 82 (2018).
- [79] C. Bressler and M. Chergui, Molecular structural dynamics probed by ultrafast x-ray absorption spectroscopy, *Annu. Rev. Phys. Chem.* **61**, 263 (2010).